viruses

MDPI

Communication

SARS-CoV-2 Error Catastrophe Under Molnupiravir: Mutagenic Enhancement Enables Viral Persistence with Impaired Fitness

Yuriko Tomita [1,*], Kaya Miyazaki [2], Rika Mochizuki [2] and Hideki Hasegawa [1,3]

[1] Influenza Research Center, National Institute of Infectious Diseases, Japan Institute of Health and Security (JIHS), Tokyo 208-0011, Japan
[2] Department of Respiratory Viruses, National Institute of Infectious Diseases, Japan Institute of Health and Security (JIHS), Tokyo 208-0011, Japan
[3] Institute for Vaccine Research and Development, Hokkaido University, Sapporo 001-0021, Japan
* Correspondence: tomita.y@jihs.go.jp; Tel.: +81-42-848-7166

Abstract

Molnupiravir induces mutations that render severe acute respiratory syndrome coronavirus 2 (SARS-CoV-2) replication-competent through error catastrophe mechanisms. Previous studies showed no resistant virus emergence during prolonged molnupiravir treatment, with no resistant variants reported. However, these approaches were limited by genetic uniformity at passage initiation. To investigate viral population dynamics under enhanced genetic diversity, we employed mutagenic pre-treatment using 5-fluorouracil (5-FU) and favipiravir to generate diverse quasi-species populations before molnupiravir selection pressure. Viral populations were treated with stepwise increasing molnupiravir concentrations (10 μM ⟶ 25 μM ⟶ 40 μM) over ten serial passages. Viral detectability, plaque morphology, and mutation accumulation were analyzed using molecular and sequencing approaches. Only high-concentration favipiravir (1000 μM) pre-treatment maintained detectable viral RNA through ten passages under 40 μM molnupiravir, while favipiravir (500 μM) and 5-FU groups became undetectable after passage 6. Surviving populations formed extremely small plaques with markedly reduced replication capacity. Next-generation sequencing revealed extensive mutation accumulation across viral proteins, including polymerase proteins. Individual viable virus isolation was unsuccessful, and large-scale propagation could not be achieved. These findings demonstrate apparent survival rather than true resistance to molnupiravir, characterized by severely compromised viral fitness.

Keywords: SARS-CoV-2; quasi-species; molnupiravir; error catastrophe; viral fitness

Check for updates

Academic Editors: Jaquelin P. Dudley and Eric O. Freed

Received: 9 January 2026
Revised: 5 February 2026
Accepted: 20 February 2026
Published: 23 February 2026

Copyright: © 2026 by the authors. Licensee MDPI, Basel, Switzerland. This article is an open access article distributed under the terms and conditions of the Creative Commons Attribution (CC BY) license.

1. Introduction

Since its emergence, severe acute respiratory syndrome coronavirus 2 (SARS-CoV-2) has demonstrated remarkable evolutionary patterns that distinguish it from most RNA viruses. Most RNA viruses utilize RNA-dependent RNA polymerase (RdRp) that lacks proofreading function, resulting in high mutation rates that enable rapid adaptation but limit genomic integrity. However, coronaviruses and other members of the Nidovirales order represent notable exceptions among RNA viruses possessing sophisticated proofreading mechanisms that allow them to maintain larger, more stable genomes while maintaining evolutionary flexibility [1,2].

This difference becomes evident when comparing mutation rates across viral families. While most RNA viruses exhibit mutation rates ranging from 10^{-6} to 10^{-4} substitu-

tions/site/year [3], the proofreading mechanisms in coronavirus result in markedly lower rates. In natural populations, SARS-CoV-2 shows evolutionary rates of 0.81–1.08 $\times$ 10^{-3} substitutions/site/year [4,5] compared to influenza A virus (4.84 $\times$ 10^{-3} substitutions/site/year) [6], representing approximately one-quarter of the rate of influenza A virus. Laboratory studies further confirm this enhanced replication fidelity, with SARS-CoV-2 demonstrating 24-fold lower mutation rates per replication cycle than influenza A virus [7].

This relatively low mutation rate is attributed to the 3′-5′ exonuclease activity of non-structural protein 14 (nsp14), whose activity is significantly enhanced (260-fold) through complex formation with the nsp10 co-factor [8]. This nsp14 exonuclease exhibits proof-reading activity that removes nucleotides incorporated with error during RNA synthesis, enabling high replication fidelity compared to other RNA viruses [9,10]. However, the proofreading function presents significant challenges for antiviral drug development. Conventional nucleoside analogs that inhibit viral RNA synthesis can be removed by the coronavirus nsp14 exonuclease after their incorporation into the viral genome, substantially reducing therapeutic efficacy [11]. Despite these challenges, nucleoside-based RdRp inhibitors remain crucial therapeutic options, with remdesivir [12] and molnupiravir [13] currently approved against SARS-CoV-2.

Molnupiravir has been approved in multiple countries as an oral therapeutic agent for patients with mild to moderate COVID-19 [14]. Unlike conventional nucleoside analogs, molnupiravir is a prodrug of a cytidine analog that is converted intracellularly to EIDD-1931, phosphorylated to EIDD-1931-TP, and incorporated by viral RdRp in place of cytidine or uridine [15]. Importantly, molnupiravir does not initiate chain termination, allowing continued RNA synthesis with incorporated errors [16]. Once integrated into viral RNA, the nsp14 exonuclease cannot completely remove all molnupiravir-containing nucleotides [16]. This misincorporation increases mutation rates beyond the lethal threshold, inducing error catastrophe [17,18], where lethal errors accumulate due to loss of genetic fidelity, leading to viral population extinction [16]. However, resistance mechanisms to this unique mode of action remain poorly understood.

Previous resistance studies have relied on spontaneous mutations arising under drug selection pressure using relatively homogenous laboratory strains [7,19]. This approach is inherently limited by genetic uniformity at the initiation of passage, restricting the pool of selectable mutations. Furthermore, reducing the sample size during serial passages poses a risk of losing potentially advantageous mutations [20]. Unlike conventional nucleoside analogs, where resistance typically involves target-specific mutations in nsp12 (RdRp) [11,21], molnupiravir's non-specific error catastrophe mechanism suggests unique resistance patterns that may not be captured by traditional approaches.

To address these limitations, this study employed a novel experimental approach by introducing genetic diversity into viral genomes prior to drug selection. Specifically, viruses were pre-treated with 5-fluorouracil (5-FU) [9,22] or favipiravir [23] as mutagenic agents to artificially create quasi-species populations with enhanced genetic diversity. These agents induce specific transition mutations—GA and UC transitions through 5-FU conversion to 5-fluorouridine triphosphate, and CU and GA transitions through favipiravir acting as a purine nucleoside analog—thereby reproducing the genetic diversity present in natural viral populations and enhancing the efficacy of detecting resistance-conferring mutations. This study presents a proof-of-concept for investigating resistance mechanisms against lethal mutagenesis-based antivirals such as molnupiravir, specifically testing whether enhanced genetic diversity enables viral persistence at the edge of error catastrophe rather than facilitating the emergence of genetically resistant viral variants.

2. Materials and Methods

2.1. Virus and Cell Culture

SARS-CoV-2 (strain WK-521) was propagated in VeroE6/TMPRSS2 cells (JCRB Cell Bank, Tsukuba, IJapan) maintained in Dulbecco's modified Eagle medium (DMEM) supplemented with 10% fetal bovine serum (FBS), 100 U/mL penicillin, and 100 μg/mL streptomycin. All virus work was conducted in a biosafety level 3 facility following institutional guidelines.

2.2. Mutagen Pre-Treatment

SARS-CoV-2 was treated with mutagenic agents to generate quasi-species populations before molnupiravir selection. Five-fluorouracil (5-FU; F6627, Sigma-Aldrich, St. Louis, MO, USA) was used at 100 μM, while favipiravir (HY14768, MedChemExpress [MCE], Monmouth Junction, NJ, USA) was used at 1000 μM or 500 μM concentrations. Virus stocks (multiplicity of infection [MOI] 0.01) were co-cultured with mutagens in VeroE6/TMPRSS2 cells for 48 h at 37 °C with 5% CO_2. Supernatants were harvested and passed once to amplify the virus groups treated with mutagens and then used for subsequent molnupiravir selection.

2.3. Molnupiravir Selection Pressure

Pre-treated virus populations were subjected to serial passage under gradually increasing molnupiravir (HY-135853, MCE) concentrations. In the initial passages (P1–P2) 10 μM of molnupiravir was used, in the intermediate passages (P3–P4) 25 μM was used, and in the final passages (P5–P10) 40 μM was used. While the 40 μM molnupiravir concentration exceeds therapeutic plasma NHC levels (~19 μM), it represents a concentration lower than the intracellular NHC-TP levels (~117 μM) achieved in target cells at clinical doses [24]. Passages were performed in T75 flasks with 15 mL DMEM containing 5% FBS and appropriate molnupiravir concentrations. When cytopathic effects (CPE) were observed by daily microscopic examination, 7 mL of supernatant was stored at −80 °C, and 7 mL was used for subsequent passage at 1:1 dilution. Control experiments used equivalent volumes of DMSO as a vehicle.

2.4. Viral Titer Quantification

Viral RNA copy numbers were quantified by quantitative real-time RT-PCR (qRT-PCR) targeting the envelope (E) gene using the 5′-UTR leader sequence to detect SARS-CoV-2 subgenomic RNA and probes. Results were expressed as viral RNA copies per milliliter.

2.5. Immunofluorescence Microscopy

Infected cells were fixed with 4% paraformaldehyde, permeabilized with 0.1% Triton X-100, and blocked with Blocking One (03953-66, Nacalai, Kyoto, Japan). Primary antibodies against SARS-CoV-2 nucleocapsid protein (40143-R019, Sino Biological, Beijing, China) were used at a 1:1000 dilution overnight at 4 °C, followed by Alexa Fluor 488-conjugated secondary antibodies (A11034, Thermo Fisher Scientific, Waltham, MA, USA). Images were captured using fluorescence microscopy, Keyence BIOZERO (Keyence, Osaka, Japan).

2.6. Plaque Assay and Plaque Size Quantification

Virus populations were serially diluted and inoculated onto confluent VeroE6/TMPRSS2 cell monolayers in 12-well plates. After 1-h adsorption at 37 °C with gentle tilting every 15 min, cells were overlaid with DMED containing 1.25% carboxymethyl cellulose and 2.5% FBS. Plates were incubated for 72 h at 37 °C with 5% CO_2, then fixed and stained with 20% methanol containing 0.05% crystal violet.

Plaque sizes were quantified from crystal violet-stained images captured using the KEYENCE microscope system. Six images per sample were captured and analyzed using CellProfiler software (version 4.2.8). Plaques located at image edges and overlapping plaques that could not be clearly separated were excluded from analysis. Plaque sizes were measured in pixels and exported for statistical analysis.

2.7. Next-Generation Sequencing (NGS)

Viral RNA was extracted from passage supernatants using MagMAX Viral/Pathogen Nucleic Acid Isolation Kit (A48310, Thermo Fisher Scientific, Waltham, MA, USA). Complementary DNA synthesis and amplification were performed using SARS-CoV-2-specific primers covering nucleotide positions 55-29836 of the genome. Library preparation was performed using the QIAseq FX DNA Library UDI kit (180475, Qiagen, Hilden, Germany) according to the manufacturer's protocol.

2.8. Variants Calling and Quality Control

Sequence variants were called against the SARS-CoV-2 genome MN908947 (WK-521) using CLC Genomics Workbench 23 (Qiagen, Hilden, Germany) with stringent quality control parameters adapted from established diagnostic NGS guidelines [25]. The following thresholds were applied: a minimum coverage of 50×, a minimum read count of 10, and a minimum variant frequency of 10%. These parameters were selected to ensure reliable variant detection while minimizing sequencing artifacts in this experimental setting.

2.9. Statistical Analysis

This study represents a single experimental run ($n = 1$) designed as a proof-of-concept investigation. Viral RNA quantification represents technical replicates from the same passage supernatant. Given the exploratory nature of this study, descriptive statistics were employed for most analyses. For plaque size quantification, statistical significance was determined using the Wilcoxon rank sum test. All statistical analyses were performed using R software (version 4.5.1) via RStudio IDE version 2025.09.0, and p-values < 0.05 were considered statistically significant.

2.10. Data Availability

Next-generation sequencing data have been deposited in the NCBI Sequence Read Archive under BioProject accession number PRJNA1392097.

3. Results

3.1. Enhanced Genetic Diversity Through Mutagenic Pre-Treatment

To investigate SARS-CoV-2 population dynamics under molnupiravir selection pressure, we employed a novel mutagenic pre-treatment approach to generate genetically diverse quasi-species populations before drug selection (Figure 1). Based on cytotoxicity assays, we selected non-cytotoxic concentrations of mutagens that could effectively introduce mutations without compromising cell viability: 5-FU at 100 μM, and favipiravir at 500 μM and 1000 μM. SARS-CoV-2 strain WK-521 was treated with these mutagens for 48 h in VeroE6/TMPRSS2 cells, followed by one passage to amplify the pre-treated populations. NGS analysis confirmed modest initial genetic diversification, with 2–3 nucleotide substitutions detected in each pre-treated population compared to the parental strain (Supplementary Table S1). These genetically diversified quasi-species populations (SARS-CoV-2_Fv1000, SARS-CoV-2_Fv500, and SARS-CoV-2_5-FU) were subsequently subjected to stepwise increasing molnupiravir concentrations (10 → 25 → 40 μM) over ten serial passages (Figure 1).

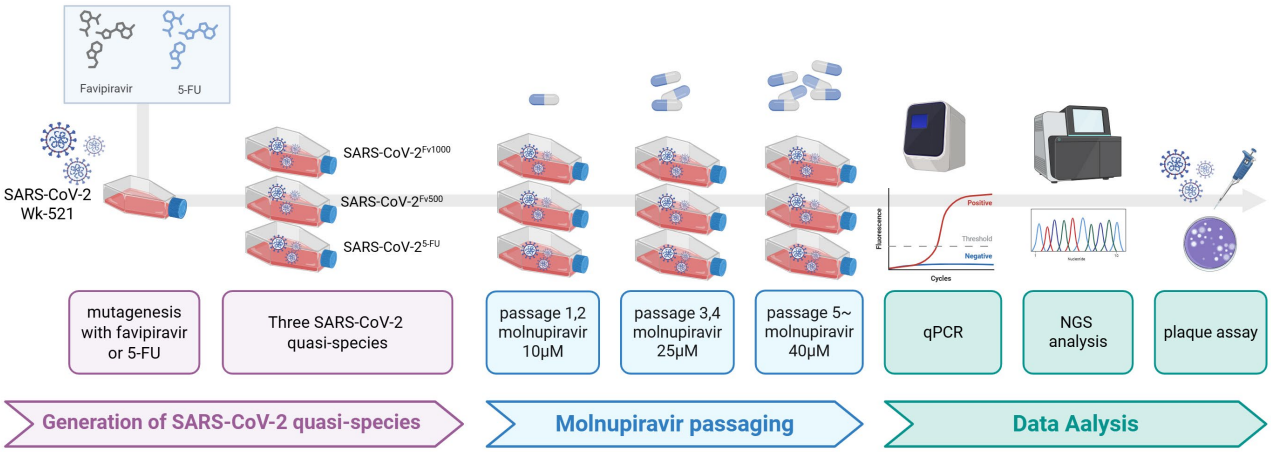


Figure 1. Experimental design for SARS-CoV-2 molnupiravir apparent resistance study. SARS-CoV-2 WK-521 was initially subjected to mutagenesis using favipiravir or 5-fluorouracil (5-FU) to generate three distinct quasi-species populations with enhanced genetic diversity. These pre-treated populations were then subjected to serial passage under gradually increasing molnupiravir concentrations: 10 μM during initial passage (P1–P2), 25 μM during intermediate passages (P3–P4), and 40 μM during final passage (P5–P10). Viral populations were maintained in T75 flasks containing DMEM with 5% FBS and appropriate drug concentrations. Passages were performed when cytopathic effects (CPE) were observed, with supernatants collected for subsequent analysis. Control passage groups without molnupiravir were generated simultaneously to assess baseline mutational patterns. Comprehensive characterisations were performed using quantitative real-time RT-PCR (qRT-PCR) for viral titer determination, next-generation sequencing (NGS) for mutational analysis, and plaque assays for viral viability assessment. Control experiments utilized equivalent DMSO volumes as vehicle controls. SARS-CoV-2^{Fv1000}: favipiravir 1000 μM pre-treated population; SARS-C-V-2^{Fv500}: favipiravir 500 μM pre-treated population; SARS-CoV-2$^{5\text{-}FU}$: 5-fluorouracil 100 μM pre-treated population. Created in BioRender. Tomita, Y. (2026) https://BioRender.com/2cfxfel (accessed on 7 January 2026).

3.2. Differential Viral Persistence Under Molnupiravir Selection

Pre-treated viral populations were subjected to stepwise increasing of molnupiravir concentrations (10 → 25 → 40 μM) over serial passage to evaluate population dynamics under drug selection pressure. qRT-PCR analysis revealed distinct survival patterns among the three pre-treated populations (Figure 2). Note that qRT-PCR quantifies detectable viral RNA rather than necessarily viable viruses. Additionally, our analysis focused on the virus released into supernatant rather than cell-associated virus, which might exhibit different mutational patterns or fitness characteristics.

The Fv1000 group (1000 μM favipiravir pre-treatment) maintained detectable viral RNA throughout all ten passages, with log10 RNA copy numbers ranging from 5.1 to 7.1, demonstrating sustained viral RNA persistence even under the highest molnupiravir concentration (40 μM). In contrast, both Fv500 (500 μM favipiravir pre-treatment) and 5-FU (100 μM 5-FU pre-treatment) groups showed comparable patterns, with detectable viral RNA levels through passage 4 (6.7 and 6.8 log10 RNA copy numbers, respectively) but became consistently undetectable from passage 6 onward.

The transition from 25 μM to 40 μM molnupiravir concentration appeared to represent a critical threshold, as only the Fv1000 population could maintain detectable levels beyond this point. All three groups showed similar RNA copy number during the initial passages (P1-P4, approximately 5.5–7.1 log10 RNA copy numbers), indicating that the differential persistence was specifically related to the higher molnupiravir concentration rather than general replication capacity differences.

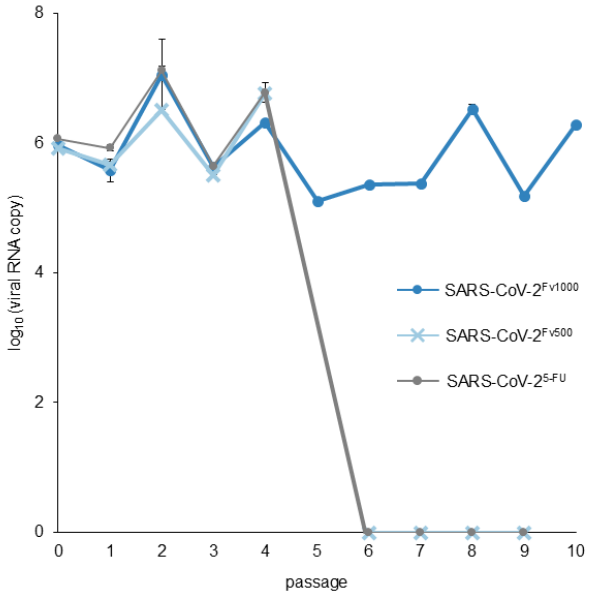


Figure 2. Viral Survival Under Molnupiravir Pressure. SARS-CoV-2 quasi-species populations pre-treated with favipiravir (1000 μM or 500 μM) or 5-fluorouracil (100 μM) were subjected to serial passage under gradually increasing molnupiravir concentrations as described in Figure 1. Viral RNA copy numbers in passage supernatants were quantified by quantitative real-time RT-PCR (qRT-PCR) targeting the envelope gene. Data represents standard deviation from technical triplicates of each passage supernatant. SARS-CoV-2^{Fv1000}: favipiravir 1000 μM pre-treated population; SARS-C-V-2^{Fv500}: favipiravir 500 μM pre-treated population; SARS-CoV-2$^{5\text{-}FU}$: 5-fluorouracil 100 μM pre-treated population.

3.3. Morphological Characteristics of Molnupiravir-Selected Viral Populations

To characterize the phenotypic properties of viral populations that persisted under molnupiravir selection pressure, we performed plaque formation assays and immunofluorescence analysis using VeroE6/TMPRSS2 cells.

Crystal violet staining revealed morphological differences between the molnupiravir-selected Fv1000_P10 population and the parental WK-521 strain (Figure 3A).

The Fv1000_P10 population produced notably smaller and irregularly shaped plaques compared to the large, well-defined circular plaques of the parental virus. The control passage maintained plaque morphology similar to the parental strain, indicating that the changes were associated with molnupiravir selection pressure.

Immunofluorescence analysis confirmed the presence of SARS-CoV-2 N protein in cells infected with the molnupiravir-selected population (Figure 3B), validating that these small plaques represented genuine viral replication. Quantitative analysis revealed a significant reduction in plaque areas for Fv1000_P10 (median: 3041 pixels^2, mean: 3170 pixels^2) compared to WK-521 (median: 15,790 pixels^2, mean: 17,281 pixels^2) ($p < 0.001$, Wilcoxon rank sum test) (Figure 3C).

Attempts to isolate individual viable viruses from the molnupiravir-selected population revealed delayed cytopathic effects appearing on day 3. qRT-PCR analysis showed Ct values above 30, indicating low viral RNA levels. Prolonged cultivation and plaque isolation attempts using limiting dilution methods were unsuccessful, as viral yields did not improve even after extended incubation periods. These findings indicate that the viral populations exhibited severely compromised replication capacity despite apparent persistence under molnupiravir selection pressure.

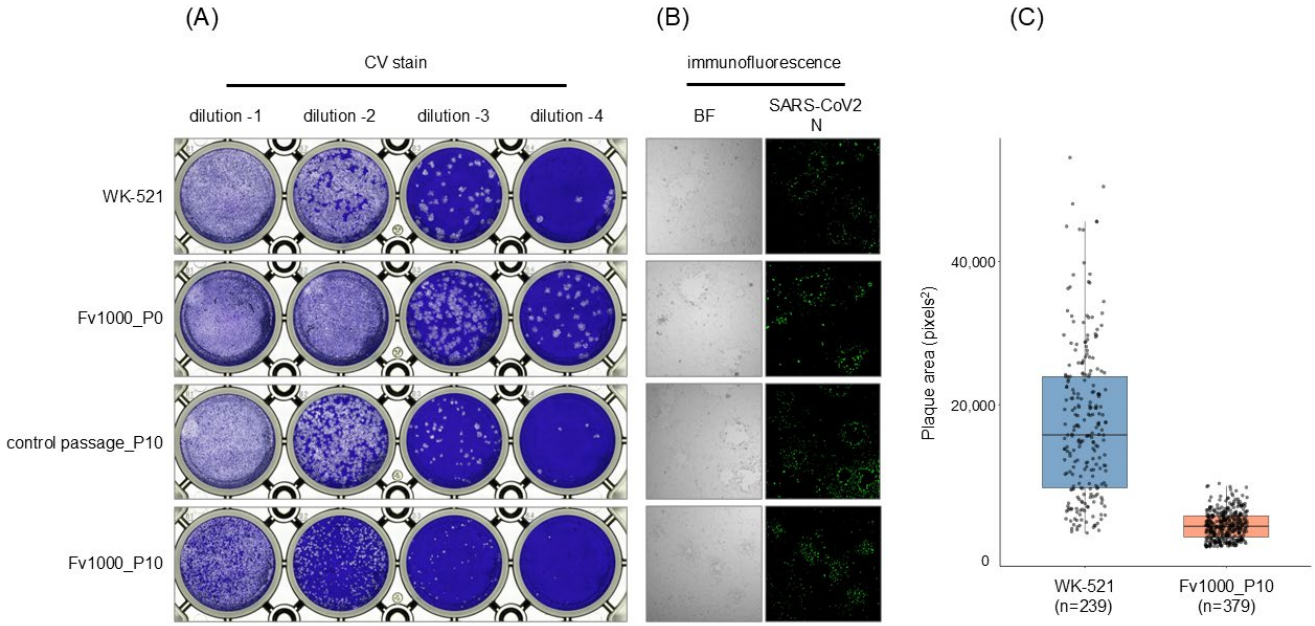


Figure 3. Morphological characteristics of SARS-CoV-2 populations under molnupiravir selection pressure. (**A**) Crystal violet staining showing plaque morphology at passage 10. Serial dilutions (1:10) of virus populations were used for plaque formation assays on VeroE6/TMPRSS2 cells. WK-521: parental strain; Fv1000_P0: virus population pre-treated with 1000 μM favipiravir before molnupiravir selection; control passage_P10: control passage without molnupiravir treatment; Fv1000_P10: virus population after 10 passages under molnupiravir selection pressure. (**B**) Immunofluorescence detection of SARS-CoV-2 nucleocapsid (N) protein in infected VeroE6/TMPRSS2 cells. Left panels show brightfield (BF) images; right panels show SARS-CoV-2 N protein staining (green fluorescence). (**C**) Quantitative analysis of plaque areas. Individual plaque areas were measured from crystal violet-stained plates. WK-521 (n = 239): parental strain plaques; Fv1000_P10 (n = 379): plaques from molnupiravir-selected population. Box plots show median, quartiles, and range. Statistical significance was determined by the Wilcoxon rank sum test ($p < 0.001$).

3.4. Extensive Mutation Accumulation Under Molnupiravir Pressure

To characterize the genetic changes occurring during molnupiravir selection, we performed a comprehensive NGS analysis of viral populations at each passage stage. Progressive mutation accumulation was observed throughout the selection process, with the Fv1000 population showing the most extensive genetic changes due to its prolonged survival under high drug concentrations (Table 1).

Table 1. Progressive mutation accumulation during serial passages with escalating molnupiravir concentrations. SARS-CoV-2 variants pretreated with mutagenic agents (Fv1000: favipiravir 1000 μM, Fv500: favipiravir 500 μM, FU: 5-FU 100 μM) were serially passaged under increasing molnupiravir concentrations. Numbers indicate synonymous (upper) and non-synonymous (lower) mutations detected at each passage (P2–P10). Control (P10) represents the same SARS-CoV-2 variants pretreated with mutagenic agents (Fv1000, Fv500, 5-FU) but passaged without molnupiravir. Total mutations are shown at the bottom of each column.

	Fv1000					**Fv500**		**5-FU**		**Control (P10)**		
	P2	**P4**	**P6**	**P8**	**P10**	**P2**	**P4**	**P2**	**P4**	**Fv1000**	**Fv500**	**5FU**
Synonymous *	5	66	55	97	89	4	36	4	53	10	17	10
Nonsynonymous	9	58	39	67	61	5	24	7	53	28	31	19
Total	14	124	94	164	150	9	60	11	106	38	48	29

Abbreviations: Fv1000/Fv500, 1000 μM or 500 μM favipiravir pre-treatment. 5-FU, 100 μM 5-FU pre-treatment. Control (P10), passage without molnupiravir.* Involve mutations identified in UTRs and intergenic regions.

The total number of mutations detected in the Fv1000 population increased dramatically from 14 mutations at passage 2 to 150 mutations by passage 10, representing more than a 10-fold increase in mutational burden. Both synonymous and non-synonymous mutations accumulated progressively, with non-synonymous changes comprising approximately 40% of total mutations across all passages. In comparison, control passages without molnupiravir pressure showed substantially lower mutation frequencies (38 total mutations at passage 10), confirming that the observed hypermutation was directly attributed to molnupiravir selection pressure rather than standard replication errors.

Analysis of nucleotide substitution patterns revealed a characteristic mutagenic signature of molnupiravir that changed with increasing drug concentration (Table 2).

Table 2. Top 5 nucleotide substitution patterns across molnupiravir concentration and control passage. Distribution of the most frequent base substitutions detected in SARS-CoV-2 under different molnupiravir selective pressures (M10: 10 μM; M25: 25 μM; M40: 40 μM) and control passage. Numbers in parentheses indicate total mutations detected.

Rank	M10 (n = 61)	M25 (n = 359)	M40 (n = 845)	Control (n = 115)
1	C → T: 32 (52.5%)	C → T: 112 (31.2%)	A → G: 250 (29.6%)	C → T: 44 (38.3%)
2	G → T: 12 (19.7%)	A → G: 92 (25.6%)	T → C: 246 (29.1%)	A → G: 20 (17.4%)
3	T → C: 9 (14.8%)	T → C: 90 (25.1%)	C → T: 220(26.0%)	G → A: 19 (16.5%)
4	T → G: 4 (6.6%)	G → A: 48 (13.4%)	G → A: 120 (14.2%)	T → C: 16 (14.0%)
5	A → G: 2 (3.3%)	G → T: 10 (2.8%)	G → T: 6 (0.7%)	G → T: 7 (6.1%)
5	G → A: 2 (3.3%)	-	-	-

At the lowest concentration (10 μM: M10 in Table 2), C ⟶ T transitions predominated (52.5%), consistent with molnupiravir's known mechanism of cytidine analog incorporation [26]. However, as molnupiravir increased to 25 μM to 40 μM (M25 and M40 in Table 2, respectively), the substitution spectrum broadened significantly, with A ⟶ G and T ⟶ C transitions becoming equally prominent (approximately 29% each at 40 μM). This shift toward more diverse substitution patterns suggests progressive disruption of replication fidelity under escalating drug pressure. Notably, the control passage maintained a more balanced substitution profile dominated by C ⟶ T and A ⟶ G changes typical of natural replication errors [27], further supporting the drug-specific nature of the observed hypermutation phenotype.

3.5. Distribution of High-Frequency Mutations in Viral Proteins Under Molnupiravir Selection

Analysis of amino acid mutations reaching ≥90% frequency by passage 10 revealed the distribution of extensive mutagenesis in multiple viral proteins (Table 3).

Under escalating molnupiravir concentrations, 38 amino acid substitutions became dominant within the viral populations, distributed across both non-structural and structural proteins.

The temporal emergence of these mutations showed a distinct pattern, with most appearing during the transition from 25 μM to 40 μM molnupiravir (passage 4–5). Many mutations that were undetectable at passage 4 suddenly appeared at a frequency of 20–30% at passage 5, then rapidly increased to dominance (>95%) by passages 6–8.

Notably, mutations were observed in critical replication machinery proteins, including the RNA-dependent RNA polymerase (nsp12) with two substitutions (Tyr458Cys, His882Arg), and the 3′-5′ exoribonuclease nsp14 responsible for proofreading activity (Ala79Val and Val182Ile). The occurrence of mutations in these essential enzymes suggests that even proteins central to viral replication fidelity were not protected from molnupiravir-induced mutagenesis. Importantly, these mutations likely represent random events during

fitness collapse rather than adaptive changes, as evidenced by the inability to isolate viable resistant variants.

Table 3. Summary of amino acid substitution with frequency ≥90% in SARS-CoV-2 following 10 passages under molnupiravir selection pressure. Only mutations detected in molnupiravir-treated cultures with frequency ≥90% at P10 are included. Mutations also present in control cultures were excluded. Molnupiravir concentrations: P1–P2 (10 μM), P3–P4 (25 μM), P5–P10 (40 μM). Numbers in parentheses indicate mutation counts for each protein. Complete mutation list with frequencies is provided in Supplementary Table S2.

Protein Category	Number of Mutations	Detected Mutations	Emergence Pattern
Replication Machinery (nsp12, nsp14)	4	nsp12 (2; Tyr458Cys, His882Arg) nsp14 (2; Ala79Val, Val182Ile)	Emerged at P4–P5, fixed by P6–P10
Protease (nsp3, nsp5)	10	nsp3 (8; Glu545Gly, etc.) nsp5 (2; Met162Val, etc.)	Concentrated emergence at P4–P5
Structural Proteins (S, N, E, M)	14	S (8; Gln218Arg, etc.), N (3), E (2), M (1)	Gradual emergence from P4–P10
Other Non-structural Proteins (nsp2, nsp4, nsp6, nsp15)	5	nsp2 (2), nsp15 (1), nsp4 (1), nsp6 (1)	Emerged at P4–P10
Accessory Proteins (ORF3a, 6, 7a, 8)	5	ORF3a (1), ORF6 (1), ORF7a (2), ORF8 (1)	Initial emergence at P4–P5
Total	38		

The highest number of mutations was observed in nsp3 (8 mutations) and the spike protein (8 mutations), while other proteins showed more limited mutational accumulation. These distribution patterns indicate that molnupiravir's mutagenic pressure affected viral proteins regardless of their structural or non-structural viral proteins.

4. Discussion

Conventional approaches to investigating antiviral resistance rely on the emergence of spontaneous mutations under drug selection pressure in genetically homogeneous laboratory strains [28–30]. This methodology presents intrinsic limitations for studying molnupiravir resistance. Unlike target-specific nucleoside analogs such as remdesivir, which develop resistance through specific mutations in the viral RNA-dependent RNA polymerase [31], molnupiravir operates through the non-specific mechanism of error catastrophe [32].

To address these constraints, we employed a mutagenic pre-treatment strategy to enhance genetic diversity prior to drug selection pressure (Figure 1). By pre-treating viral populations with 5-FU and favipiravir, we aimed to generate quasi-species populations approximating natural viral genetic diversity [26]. This proof-of-concept investigation tested whether enhanced initial genetic diversity could facilitate the emergence of molnupiravir-tolerant populations under conditions where conventional approaches have consistently failed to identify resistant variants [24]. Our results demonstrate that even under artificially enhanced genetic diversity conditions, the emergence of truly resistant SARS-CoV-2 populations remains challenging, supporting the robustness of molnupiravir's barriers to resistance development.

Our findings reveal a complex phenomenon that we term "apparent survival" rather than true resistance (Figure 2). Only the high-concentration favipiravir pre-treated population (Fv1000) maintained detectable viral RNA through ten passages under escalating molnupiravir concentrations, while other groups became undetectable after passage 6. The transition from 25 μM to 40 μM molnupiravir represents a threshold concentration, suggesting a critical point in the error catastrophe mechanism [16,30].

The persisting Fv1000_P10 population exhibited severely compromised replication capacity, forming extremely small plaques with significantly reduced areas compared

to parental virus (median: 3041 vs 15,790 pixels^2, $p < 0.001$) (Figure 3). Although immunofluorescence confirmed genuine viral replication, attempts to isolate individual viable viruses were unsuccessful, and large-scale propagation could not be achieved. These characteristics suggest a population existing at the edge of viability rather than displaying conventional resistance.

This phenomenon aligns with error catastrophe theory, where heavily mutated viral populations exist at the edge of viability, approaching but not surpassing the extinction threshold [16,33]. The extensive mutation accumulation observed (150 mutations by passage 10 versus 38 in controls) (Table 1) indicates that molnupiravir successfully induced hypermutation, yet some viral genomes retained minimal functionality. The inability to isolate individual resistant viruses suggests that survival depended on population-level complementation effects rather than individual genome fitness.

Our mutational analysis reveals a distinct dose-dependent evolution of mulnupiravir'smutagenic signature (Table 2). At the lowest concentration (10 μM), the C-to-T transition is predominant (52.5%), consistent with molnupiravir's established mechanism as a cytidine analog [10]. However, as concentrations increased, we observed a striking shift in the mutational spectrum: at 25 μM, the C-to-T frequency decreased to 31.2%, while A-to-G and T-to-C transitions increased substantially (25.6% and 25.1%, respectively). At the highest concentration (40 μM), this pattern reversed entirely, with A-to-G (29.6%) and T-to-C (29.1%) transitions becoming predominant over C-to-T (26.0%).

This concentration-dependent shift likely reflects the compound effects of multiple replication cycles under sustained mutagenic pressure, amplified by SARS-CoV-2's inherent nucleotide composition bias. The SARS-CoV-2 genome is naturally enriched in adenine and uracil residues, with our experimental strain (WK-521, MN908947) exhibiting a GC content of only 38.0%. Initial rounds of replication generate C-to-T and G-to-A transitions through molnupiravir's primary mechanism, further shifting the already A/U-rich genome toward even greater adenine thymine abundance. Subsequent replication cycles then preferentially target these accumulated A and T nucleotides for conversion to G and C, respectively, explaining the secondary surge in A-to-G and T-to-C transitions at higher drug concentrations. This interpretation is supported by Strizki et al.'s serial passage experiments, where prolonged exposure to NHC similarly generated high frequencies of A-to-G and T-to-C transitions alongside the expected C-to-T and G-to-A changes [31].

Notably, mutations accumulated even in critical replication machinery, including RNA-dependent RNA polymerase (nsp12: Tyr458Cys, His882Arg) and the proofreading exonuclease nsp14 (Ala79Val, Val182Ile) (Table 3). The viral RNA synthesis machinery consists of the core polymerase complex (nsp7, nsp8, nsp12) and the proofreading exonuclease nsp14. While no mutations were detected in nsp7 and nsp8, mutations were identified in both nsp12 and nsp14. The nsp12 mutations Y458C and H882R have not been reported in large-scale genomic analyses and are likely to represent novel variants. Y458C is predicted to be located in the fingers subdomain and H882R in the thumb subdomain of the polymerase domain. The Y458C substitution may introduce novel disulfide bond formation due to the tyrosine-to-cysteine change, while the H882R substitution may alter electrostatic interactions through the histidine-to-arginine change, potentially affecting polymerase structure and cofactor interactions. The occurrence of mutations in nsp14, which normally provides error-correction function through its N-terminal DEDD motif exonuclease activity [34], suggests that molnupiravir's mutagenic pressure can overwhelm even the coronavirus proofreading system. Notably, the identified nsp14 mutations (Ala79Val, Val182Ile) did not occur within the critical DEDD exonuclease active site, similar to the nsp12 mutations, which also avoided the polymerase active site. However, these mutations should be interpreted cautiously as they likely represent random mutational drift in a population under

severe fitness constraints rather than functional resistance mechanisms, particularly given that resistant virus isolation was not achieved in this study.

This proof-of-concept study has several important limitations. The experimental design involved a single run (n = 1), which limited statistical power and generalizability. Therefore, the specific mutational trajectories observed should be interpreted as a plausible mechanistic scenario rather than reproducible patterns, though the overall phenomenon of apparent survival under severe fitness constraints appears consistent with error catastrophe theory.

Our mutagenic pre-treatment achieved only modest detectable genetic diversification (2–3 initial mutations; Supplementary Table S1), which may reflect both sequencing coverage limitations and insufficient mutagenic pressure to fully test the hypothesis. The molnupiravir concentrations employed, particularly the final 40 μM, exceed clinically relevant plasma concentrations (~18 μM) but remain below intracellular active metabolite concentrations (~117 μM), thereby moderating concerns about translational significance [24]. Additionally, our focus on a single viral strain (WK-521) represents a limitation, as different SARS-CoV-2 variants might respond differently to similar experimental conditions [34].

Despite these limitations, our findings contribute to understanding molnupiravir's resistance barrier. The consistent failure to generate truly resistant variants, even under artificially enhanced genetic diversity, suggests that molnupiravir possesses robust intrinsic barriers to the development of resistance. Future research directions should include larger-scale validation studies, investigation of different viral strains, and examination of resistance emergence under clinically relevant drug concentrations.

5. Conclusions

This study demonstrates that even under conditions of enhanced genetic diversity, SARS-CoV-2 populations fail to develop true resistance to molnupiravir, instead exhibiting apparent survival characterized by severely compromised viral fitness. While our experimental approach successfully generated persistent viral populations under extreme selective pressure, these populations represented functionally impaired survivors rather than fit resistant variants. These findings support the robust barrier that molnupiravir presents against the development of resistance, reinforcing its potential for sustained clinical efficacy.

Supplementary Materials: The following supporting information can be downloaded at: https://www.mdpi.com/article/10.3390/v18020273/s1, Table S1: Initial mutation profile in mutagen pre-treated SARS-CoV-2 populations; Table S2: Complete list of amino acid substitutions in SARS-CoV-2 following 10 passages under molnupiravir selection pressure, including all mutations with frequencies < 90%.

Author Contributions: Y.T. conceived and designed the study, performed the experiments, analyzed the data, and wrote the original draft. K.M. and R.M. contributed to the investigation. H.H. reviewed and edited the manuscript and acquired funding with Y.T. All authors have read and agreed to the published version of the manuscript.

Funding: This work was supported by a Health and Labour Sciences Research grant (no. 24HA2005), a Japan Society for the Promotion of Science grant (23K06576) and the Japan Agency for Medical Research and Development (AMED) grant (JP223fa627005).

Institutional Review Board Statement: This study was approved by the institutional Review Board of the National Institute of Infectious Disease (protocol code 25-005 and 20251211).

Informed Consent Statement: Not applicable.

Data Availability Statement: The raw sequencing data supporting the findings of this study are available from NCBI's Sequence Read Archive (SRA) under BioProject accession number PRJNA1392097.

Acknowledgments: We are grateful to Takayama for valuable discussions regarding NGS data interpretation and to Matsuyama for valuable scientific discussions and constructive feedback on the experimental design and findings. We also thank the staff of Influenza Research Center for their valuable discussions and laboratory support. During the preparation of this manuscript, the author(s) used Claude (Claude 3.5 Sonnet, Anthropic, accessed in January 2025) for the purposes of improving clarity and consistency, and correcting grammar. The authors have reviewed and edited the output and take full responsibility for the content of this publication.

Conflicts of Interest: The authors declare no conflict of interest.

References

1. Gorbalenya, A.E.; Enjuanes, L.; Ziebuhr, J.; Snijder, E.J. Nidovirales: Evolving the Largest RNA Virus Genome. *Virus Res.* **2006**, *117*, 17–37. [CrossRef] [PubMed]
2. Denison, M.R.; Graham, R.L.; Donaldson, E.F.; Eckerle, L.D.; Baric, R.S. Coronaviruses: An RNA Proofreading Machine Regulates Replication Fidelity and Diversity. *RNA Biol.* **2011**, *8*, 270–279. [CrossRef]
3. Peck, K.M.; Lauring, A.S. Complexities of Viral Mutation Rates. *J. Virol.* **2018**, *92*, 10–1128. [CrossRef]
4. Pereson, M.J.; Flichman, D.M.; Martínez, A.P.; Baré, P.; Garcia, G.H.; Di Lello, F.A. Evolutionary Analysis of SARS-CoV-2 Spike Protein for Its Different Clades. *J. Med. Virol.* **2021**, *93*, 3000–3006. [CrossRef]
5. Wang, S.; Xu, X.; Wei, C.; Li, S.; Zhao, J.; Zheng, Y.; Liu, X.; Zeng, X.; Yuan, W.; Peng, S. Molecular Evolutionary Characteristics of SARS-CoV-2 Emerging in the United States. *J. Med. Virol.* **2022**, *94*, 310–317. [CrossRef]
6. Kim, J.I.; Lee, I.; Park, S.; Bae, J.-Y.; Yoo, K.; Cheong, H.J.; Noh, J.Y.; Hong, K.W.; Lemey, P.; Vrancken, B.; et al. Phylogenetic Relationships of the HA and NA Genes between Vaccine and Seasonal Influenza A(H3N2) Strains in Korea. *PLoS ONE* **2017**, *12*, e0172059. [CrossRef]
7. Kawasaki, Y.; Abe, H.; Yasuda, J. Comparison of Genome Replication Fidelity between SARS-CoV-2 and Influenza A Virus in Cell Culture. *Sci. Rep.* **2023**, *13*, 13105. [CrossRef] [PubMed]
8. Riccio, A.A.; Sullivan, E.D.; Copeland, W.C. Activation of the SARS-CoV-2 NSP14 3′-5′ Exoribonuclease by NSP10 and Response to Antiviral Inhibitors. *J. Biol. Chem.* **2022**, *298*, 101518. [CrossRef] [PubMed]
9. Smith, E.C.; Blanc, H.; Surdel, M.C.; Vignuzzi, M.; Denison, M.R. Coronaviruses Lacking Exoribonuclease Activity Are Susceptible to Lethal Mutagenesis: Evidence for Proofreading and Potential Therapeutics. *PLoS Pathog.* **2013**, *9*, e1003565. [CrossRef]
10. Tahir, M. Coronavirus Genomic Nsp14-ExoN, Structure, Role, Mechanism, and Potential Application as a Drug Target. *J. Med. Virol.* **2021**, *93*, 4258–4264. [CrossRef]
11. Stevens, L.J.; Pruijssers, A.J.; Lee, H.W.; Gordon, C.J.; Tchesnokov, E.P.; Gribble, J.; George, A.S.; Hughes, T.M.; Lu, X.; Li, J.; et al. Distinct Genetic Determinants and Mechanisms of SARS-CoV-2 Resistance to Remdesivir. *bioRxiv* **2022**.
12. Beigel, J.H.; Tomashek, K.M.; Dodd, L.E.; Mehta, A.K.; Zingman, B.S.; Kalil, A.C.; Hohmann, E.; Chu, H.Y.; Luetkemeyer, A.; Kline, S.; et al. Remdesivir for the Treatment of Covid-19 - Final Report. *N. Engl. J. Med.* **2020**, *383*, 1813–1826. [CrossRef]
13. Jayk Bernal, A.; Gomes da Silva, M.M.; Musungaie, D.B.; Kovalchuk, E.; Gonzalez, A.; Delos Reyes, V.; Martín-Quirós, A.; Caraco, Y.; Williams-Diaz, A.; Brown, M.L.; et al. Molnupiravir for Oral Treatment of Covid-19 in Nonhospitalized Patients. *N. Engl. J. Med.* **2022**, *386*, 509–520. [CrossRef]
14. CDC COVID-19 Treatment Clinical Care for Outpatients. Available online: https://www.cdc.gov/covid/hcp/clinical-care/outpatient-treatment.html (accessed on 10 September 2025).
15. Maas, B.M.; Strizki, J.; Miller, R.R.; Kumar, S.; Brown, M.; Johnson, M.G.; Cheng, M.; De Anda, C.; Rizk, M.L.; Stone, J.A. Molnupiravir: Mechanism of Action, Clinical, and Translational Science. *Clin. Transl. Sci.* **2024**, *17*, e13732. [CrossRef] [PubMed]
16. Kabinger, F.; Stiller, C.; Schmitzová, J.; Dienemann, C.; Kokic, G.; Hillen, H.S.; Höbartner, C.; Cramer, P. Mechanism of Molnupiravir-Induced SARS-CoV-2 Mutagenesis. *Nat. Struct. Mol. Biol.* **2021**, *28*, 740–746. [CrossRef] [PubMed]
17. Crotty, S.; Cameron, C.E.; Andino, R. RNA Virus Error Catastrophe: Direct Molecular Test by Using Ribavirin. *Proc. Natl. Acad. Sci. USA* **2001**, *98*, 6895–6900. [CrossRef]
18. Holmes, E.C. Error Thresholds and the Constraints to RNA Virus Evolution. *Trends Microbiol.* **2003**, *11*, 543–546. [CrossRef]
19. Strizki, J.M.; Gaspar, J.M.; Howe, J.A.; Hutchins, B.; Mohri, H.; Nair, M.S.; Kinek, K.C.; McKenna, P.; Goh, S.L.; Murgolo, N. Molnupiravir Maintains Antiviral Activity against SARS-CoV-2 Variants and Exhibits a High Barrier to the Development of Resistance. *Antimicrob. Agents Chemother.* **2024**, *68*, e0095323. [CrossRef] [PubMed]
20. Yuste, E.; López-Galíndez, C.; Domingo, E. Unusual Distribution of Mutations Associated with Serial Bottleneck Passages of Human Immunodeficiency Virus Type 1. *J. Virol.* **2000**, *74*, 9546–9552. [CrossRef]

21. Hu, Y.; Lewandowski, E.M.; Tan, H.; Zhang, X.; Morgan, R.T.; Zhang, X.; Jacobs, L.M.C.; Butler, S.G.; Gongora, M.V.; Choy, J.; et al. Naturally Occurring Mutations of SARS-CoV-2 Main Protease Confer Drug Resistance to Nirmatrelvir. *ACS Cent. Sci.* **2023**, *9*, 1658–1669. [CrossRef]
22. de la Higuera, I.; Ferrer-Orta, C.; de Ávila, A.I.; Perales, C.; Sierra, M.; Singh, K.; Sarafianos, S.G.; Dehouck, Y.; Bastolla, U.; Verdaguer, N.; et al. Molecular and Functional Bases of Selection against a Mutation Bias in an RNA Virus. *Genome Biol. Evol.* **2017**, *9*, 1212–1228. [CrossRef]
23. Shannon, A.; Selisko, B.; Le, N.T.T.; Huchting, J.; Touret, F.; Piorkowski, G.; Fattorini, V.; Ferron, F.; Decroly, E.; Meier, C.; et al. Rapid incorporation of Favipiravir by the fast and permissive viral RNA polymerase complex results in SARS-CoV-2 lethal mutagenesis. *Nat. Commun.* **2020**, *11*, 4682. [CrossRef] [PubMed]
24. Nakamura, K.; Fujimoto, K.; Hasegawa, C.; Aoki, I.; Yoshitsugu, H.; Ugai, H.; Yatsuzuka, N.; Tanaka, Y.; Furihata, K.; Maas, B.M.; et al. A Phase I, Randomized, Placebo-Controlled Study of Molnupiravir in Healthy Japanese to Support Special Approval in Japan to Treat COVID-19. *Clin. Transl. Sci.* **2022**, *15*, 2697–2708. [CrossRef]
25. Petrackova, A.; Vasinek, M.; Sedlarikova, L.; Dyskova, T.; Schneiderova, P.; Novosad, T.; Papajik, T.; Kriegova, E. Standardization of Sequencing Coverage Depth in NGS: Recommendation for Detection of Clonal and Subclonal Mutations in Cancer Diagnostics. *Front. Oncol.* **2019**, *9*, 851. [CrossRef]
26. Hadj Hassine, I.; Ben M'hadheb, M.; Menéndez-Arias, L. Lethal Mutagenesis of RNA Viruses and Approved Drugs with Antiviral Mutagenic Activity. *Viruses* **2022**, *14*, 841. [CrossRef] [PubMed]
27. Lauring, A.S.; Andino, R. Quasispecies Theory and the Behavior of RNA Viruses. *PLoS Pathog.* **2010**, *6*, e1001005. [CrossRef]
28. Kiso, M.; Yamayoshi, S.; Iida, S.; Furusawa, Y.; Hirata, Y.; Uraki, R.; Imai, M.; Suzuki, T.; Kawaoka, Y. In Vitro and in Vivo Characterization of SARS-CoV-2 Resistance to Ensitrelvir. *Nat. Commun.* **2023**, *14*, 4231. [CrossRef]
29. Stevens, L.J.; Pruijssers, A.J.; Lee, H.W.; Gordon, C.J.; Tchesnokov, E.P.; Gribble, J.; George, A.S.; Hughes, T.M.; Lu, X.; Li, J.; et al. Mutations in the SARS-CoV-2 RNA-Dependent RNA Polymerase Confer Resistance to Remdesivir by Distinct Mechanisms. *Sci. Transl. Med.* **2022**, *14*, eabo0718. [CrossRef]
30. Jochmans, D.; Liu, C.; Donckers, K.; Stoycheva, A.; Boland, S.; Stevens, S.K.; De Vita, C.; Vanmechelen, B.; Maes, P.; Trüeb, B.; et al. The Substitutions L50F, E166A, and L167F in SARS-CoV-2 3CLpro Are Selected by a Protease Inhibitor In Vitro and Confer Resistance To Nirmatrelvir. *MBio* **2023**, *14*, e0281522. [CrossRef]
31. Kokic, G.; Hillen, H.S.; Tegunov, D.; Dienemann, C.; Seitz, F.; Schmitzova, J.; Farnung, L.; Siewert, A.; Höbartner, C.; Cramer, P. Mechanism of SARS-CoV-2 Polymerase Stalling by Remdesivir. *Nat. Commun.* **2021**, *12*, 279. [CrossRef] [PubMed]
32. Malone, B.; Campbell, E.A. Molnupiravir: Coding for Catastrophe. *Nat. Struct. Mol. Biol.* **2021**, *28*, 706–708. [CrossRef] [PubMed]
33. Sanderson, T.; Hisner, R.; Donovan-Banfield, I.; Hartman, H.; Løchen, A.; Peacock, T.P.; Ruis, C. A Molnupiravir-Associated Mutational Signature in Global SARS-CoV-2 Genomes. *Nature* **2023**, *623*, 594–600. [CrossRef] [PubMed]
34. Baniecki, M.L.; Guan, S.; Rai, D.K.; Yang, Q.; Lee, J.T.; Hao, L.; Weinstein, E.; Hyde, C.; Cardin, R.D.; Soares, H.; et al. Integrated Virologic Analysis of Resistance to Nirmatrelvir/Ritonavir in Individuals across Four Phase 2/3 Clinical Studies for the Treatment of COVID-19. *EBioMedicine* **2025**, *118*, 105819. [CrossRef] [PubMed]

Disclaimer/Publisher's Note: The statements, opinions and data contained in all publications are solely those of the individual author(s) and contributor(s) and not of MDPI and/or the editor(s). MDPI and/or the editor(s) disclaim responsibility for any injury to people or property resulting from any ideas, methods, instructions or products referred to in the content.